MODELLING OF TWO-PHASE FLOW IN POROUS MEDIA INCLUDING NON-EQUILIBRIUM CAPILLARY PRESSURE EFFECTS

BERENTSEN, C.W.J.[1], S.M. HASSANIZADEH[1], A. BEZUIJEN[2] O. OUNG[2]

[1]*Utrecht University, Department of Earth Sciences, Environmental Hydrogeology group, Budapestlaan 4, 3508 TA, Utrech, The Netherlands*
[2]*GeoDelft, Stieltjesweg 2, 2628 CK, Delft, The Netherlands*

Abstract

Two-phase flow models commonly use equilibrium capillary-pressure relations in which the capillary pressure is a function of saturation only. However, even in core-scale experiments, the time needed to reach capillary equilibrium is in the order of days if not weeks. Therefore, the question arises whether equilibrium capillary-pressure relation is valid for modelling dynamic flow problems. Some recently developed theories account for non-equilibrium capillary pressure effects at the macro-scale, by proposing that capillary pressure is a function of saturation rate.

In this study, we investigated the necessity to account for non-equilibrium capillary pressure effects at the local scale. Recently we have carried out a number of two-phase drainage experiments. The experimental data clearly indicate the existence of a local non-equilibrium effect. We tried to simulate our experimental data using the non-equilibrium two-phase flow model.

We developed a numerical code in which we simultaneously solve for the wetting phase saturation, wetting phase pressure and non-wetting phase pressure by solving the flow equations and the non-equilibrium capillary pressure relation. Next the numerical model is compared to the data of the non-equilibrium two-phase flow experiments. We find that the data cannot be modelled without inclusion of the non-equilibrium effect. Reasonably good agreement with data is obtained when the non-equilibrium capillary pressure term is included.

1. Introduction

In two-phase flow models the capillary pressure-saturation relationship is traditionally modelled as an equilibrium process. However, even in core-scale experiments, the time needed to reach capillary-gravity equilibrium is already in the order of many days to weeks. Therefore, potentially, under transient flow conditions, non-equilibrium effects in capillary pressure-saturation curves need to be taken into account.

In recent years, there has been increasing interest on the significance of non-equilibrium capillary pressure effects for unsaturated and two-phase flow problems. There exist theories that account for non-equilibrium capillary pressure at the (upscaled) macro scale, by proposing that capillary pressure to be a function of saturation rate of change as well as saturation (Barenblatt et al. 1987, Hassanizadeh and Gray 1990). These theories result in a capillary pressure that is larger than the equilibrium capillary pressure in case of drainage and

smaller in case of imbibition. In unsaturated porous media, there is indeed ample experimental evidence on the existence and more importantly the significance of these non-equilibrium effects (see Hassanizadeh et al. for a review). However, there are very few experiments dealing with two-phase flow.

Recently we have carried out a number of two-phase flow experiments consisting of both drainage and imbibition in a small column set-up. The experimental data indicate the existence of a local non-equilibrium capillary pressure effect.

In this manuscript, we describe our experiments, present the data, and investigate the significance of non-equilibrium capillary pressure effects at the local scale. We try to simulate experimental data using a model that includes the non-equilibrium capillary pressure effect.

2. Two-phase flow model

At the macroscopic or REV scale, the governing equations for two-phase incompressible flow are the mass balance for each phase α (Helmig, 1997).

$$\frac{\partial S^{\alpha}}{\partial t} + \frac{1}{\phi}\nabla \bullet \mathbf{u}_{\alpha} = 0 \tag{1}$$

and Darcy's law stating the relation between the Darcy phase velocity ($\mathbf{u}_{\alpha}$) and the driving phase potential Φ^{α}, defined by $\nabla\Phi^{\alpha} = \nabla p^{\alpha} + \rho^{\alpha} g \mathbf{e}_z$:

$$\mathbf{u}_{\alpha} = -\Lambda_{\alpha}\nabla\Phi^{\alpha}, \qquad \Lambda_{\alpha} = K k_r^{\alpha} / \mu^{\alpha} \tag{2}$$

Here, S is the saturation, K is the intrinsic permeability tensor, Λ is the mobility, k_r is the relative permeability, μ is the viscosity, ρ is the density, ϕ is the porosity, g is the gravitational acceleration and z is the elevation. By definition the phase saturations add up to 1:

$$S^n + S^w = 1 \tag{3}$$

In addition to (1) and (2), we need an equation that relates the pressures of the two phases.

Classically the local macroscopic capillary pressure is defined as a (static) equilibrium relation between the non-wetting phase and water pressure differences:

$$p^n - p^w = p_c\left(S^w\right) \tag{4}$$

in which the static capillary pressure function p_{stat}^c is assumed to be a unique function of the saturation. We assume that Brooks-Corey formula prescribes the capillary pressure relation:

$$p_c(S^e) = p_d (S^e)^{-1/\lambda} \tag{5}$$

Here, p_d is the entry pressure, λ is the sorting factor and

$$S^e = (S^w - S_{res}^w)/(1 - S_{res}^w - S_{res}^n) \tag{6}$$

is the effective wetting phase saturation. In (6), S_{res}^w is the residual wetting phase saturation and S_{res}^n is the residual non-wetting phase saturation, which is assumed to be zero in this study.

In this article, we investigate the following local non-equilibrium relation (after Hassanizadeh and Gray, 1993)

$$p^n - p^w = p_c(S^w) - \tau(S^w)\frac{\partial S^w}{\partial t} \tag{7}$$

in which the difference in phase pressures also depends on the temporal change of saturation.

Relative permeabilities for the wetting phase and non-wetting phase are assumed to be directly related to the static capillary pressure function:

$$k_r^w = (S^e)^{(2+3\lambda)/\lambda}$$
$$k_r^n = \left(1-(S^e)^2\right)\left(1-(S^e)^{(2+\lambda)/\lambda}\right) \quad (8)$$

In the present study, we strictly focus on the non-equilibrium effects within the capillary pressure and ignore possible non-equilibrium effects in the relative permeability curves.

3. Experimental set-up

Here, a brief description of the experimental set-up is provided. More details can be found in Hassanizadeh et al. (2004). An initially water saturated sand sample of 3cm in height and 6 cm in diameter is placed in between a PCE reservoir separated by a hydrophobic membrane (top) and a water reservoir separated by a hydrophilic membrane (bottom) (see Fig 1). The top membrane prevents water from entering the PCE reservoir. The hydrophilic bottom membrane prevents PCE entering the water reservoir. The membranes (of 125μm thickness) are supported by highly porous and permeable brass filters with a thickness of 0.9cm. Pressurizing the PCE reservoir (pressure measured by increasing the sensor N-out) causes PCE to invade the soil as soon as the sand entry pressure is overcome. The PCE entering the sand from the top pushes the water through the bottom into the water reservoir. Water leaving the set-up accumulates in a Burette connected to the water reservoir. The sensor W-out in the water reservoir measures the increase in water volume in the Burette. A hydrophilic pressure sensor (W-in) measures the water pressure inside the sand sample, whereas a hydrophobic sensor (N-in) measures PCE pressure inside the sample. These interior sensors are in contact with the sand over an area of 7 mm in diameter.

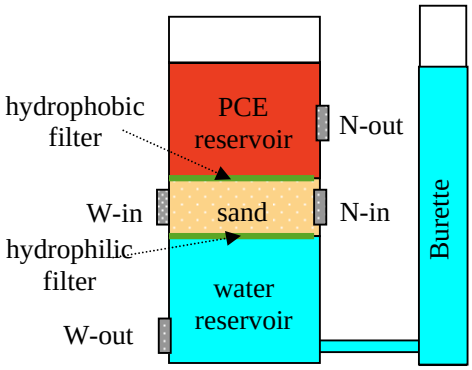

FIGURE 1. Experimental set-up

4. Experimental results

Static and non-equilibrium capillary pressure experiments have been performed in a temperature controlled room. The static experiment is required to determine the Brooks Corey coefficients that are used in the evaluation of the dynamic experiments.

4.1 Determination of static $p^c - S^w$ relationships

In the "static" drainage experiments, the P_{N-out} pressure is increased incrementally by small steps each time equilibrium has been established. Equilibrium is assumed to have been reached when the temporal change in saturation becomes negligibly small. As mentioned above, the average saturation of the sample is measured volumetrically. The pressures of wetting and non-wetting fluids are measured in the bottom and top reservoirs p_{W-out} and p_{N-out}, respectively. One may calculate the static capillary pressure distribution inside the sample by assuming a linear pressure distribution for each phase within the sample, so that:

$$p_i^c(z) = p_{N-out} - p_{W-out} + \rho^n g h_{N-out} + (\rho^w - \rho^n) g z \tag{9}$$

where z is the elevation measured from the location of the *W-out* transducer and h_{N-out} is the elevation of the *N-out* transducer. Knowing p_i^c from (9), the saturation distribution inside the sand sample, $S^w(z)$ is determined by inverting the static relation (5) for any given triple {entry pressure p^d, connate water saturation S_{res}^w, sorting coefficient λ}. We look for the set of coefficients $\{p^d, S_{res}^w, \lambda\}$ that minimizes the sum of square of differences between the measured averaged water saturations and the computed sample-averaged water saturations. Hence it minimizes the objective function:

$$O = \sum_{i=1}^{\#measurements} \left(\left\langle S_i^w \right\rangle - \frac{1}{L} \int_0^L S_i^{w*} \left(p_i^c(z); \lambda, S_{res}^w, p^d \right) dz \right)^2 \tag{10}$$

The objective function appeared to be smooth and we obtained p^d=5900 Pa, λ=6.27 and S_{res}^w=0.107 as the optimal values. For these values, Fig 2 compares the data with the static model [equations (1), (2), and (5)] through the exterior capillary pressure $p_{out}^c = p_{N-out} - p_{W-out}$ and interior capillary pressure $p_{in}^c = p_{N-in} - p_{W-in}$ as function of the averaged saturation. Fig 2 shows a good fit between model and data.

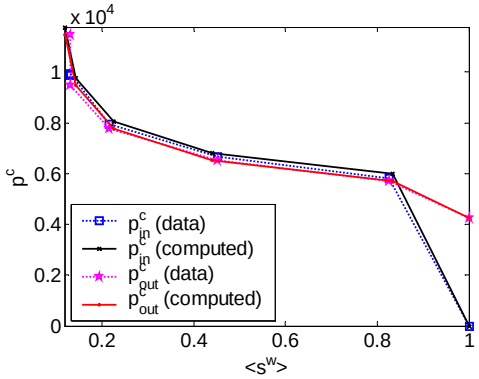

FIGURE 2: Comparison of the measured (data) and computed (9) interior capillary pressure $p_{in}^c = p_{in}^n - p_{in}^w$ and exterior capillary pressure $p_{out}^c = p_{N-out} - p_{w-out}$ as function of the averaged saturation $< S^w >$.

4.2 Non-equilibrium p^c-S^w curves

In three non-equilibrium experiments, the DNAPL pressure (p_{N-out}) was instantaneously raised by $\Delta P = 16$, 20, or 25 kPa. PCE and water pressures (p_{N-in} and p_{W-in}) as well as the saturation change of the sample were measured as a function of time. This data was then used to plot the dynamic capillary pressure p_{in}^c as a function of time (Fig. 3a) as well as a function of the sample saturation (Fig. 3b). The p^c-S^w curves start at a saturation less than unity because it takes time for the drainage front to reach the transducers while the sample saturation start to decrease immediately after the start of the experiment. In all three experiments, we see a non-monotonous behavior of the capillary pressure curve (p_{in}^c) in both Figs 3a and 3b. In Fig. 3b, in agreement with the non-equilibrium relation (7), the 20kPa and 25kPa show a significantly larger overshoot than the 16kPa experiment. One may further observe that in the time range $t \in [50, 100]$, the capillary pressure in the 25-kPa experiment is significantly larger than the capillary pressure of the other experiments. In a relative sense the arrival time of the DNAPL at the interior sensors appears to be the fastest in the 20kPa experiment followed by the 25 kPa and 16 kPa cases.

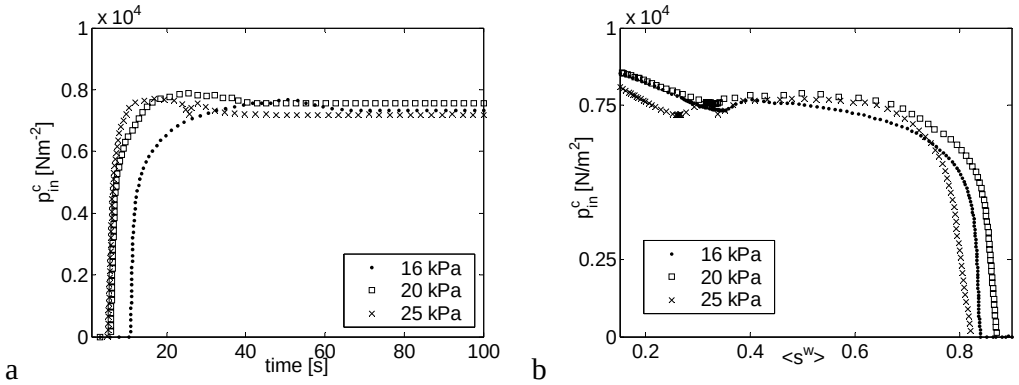

a b

FIGURE 3. Dynamic capillary pressures plotted as a function of time and saturation

5. Numerical model

In our one-dimensional (1D) numerical model, we solve the following set of equations for the non-wetting phase saturation S^n and the two phase potentials Φ^n and Φ^w, simultaneously:

$$\begin{aligned} &+\phi \partial_t S^n - \nabla(\Lambda^n \nabla \Phi^n) = 0 \\ &-\phi \partial_t S^n - \nabla(\Lambda^w \nabla \Phi^w) = 0 \\ &\Phi^n - \Phi^w - [\rho^n - \rho^w] gz = p_c\left(S^n\right) + \tau(S^n)\partial_t S^n \end{aligned} \tag{11}$$

We solve (11) iteratively using the implicit Newton-Raphson method. We use the standard first order discretization scheme in which the phase relative permeabilities are first order upwind weighted. The time step used is variable and is constrained by a maximum allowable saturation change of 0.1 per grid block per time step.

The computational domain comprises the combined brass filter / membranes at the bottom and top and the sand sample of 3cm. To allow for grid blocks larger than the membrane

thickness of 125μm, we assign each filter/membrane a length of 1 *cm* and an equivalent transmissivity.

Initially the sand and membrane/filter at the bottom are fully water saturated while the top filter/membrane is assumed to be saturated with DNAPL for 99.9%. At the top boundary, a no-flux boundary is imposed for the water phase and the DNAPL pressure is prescribed according to the experimentally measured (Dirichlet B.C.):

$$p^n_{top}(t) = p_{N-out}(t) + (z_{top} - z_{N-out})\rho^n g, \qquad q^w_{top} = 0 \tag{12}$$

At the bottom, no DNAPL flow is imposed. The bottom boundary condition for the water phase is a mixed condition that accounts for the increasing hydrostatic pressure resulting from the accumulation of water volume in the Burette:

$$\frac{1}{\rho^w g}\frac{\partial p^w_{bottom}}{\partial t} = \mid u^w_{bottom} \mid \frac{A_{sample}}{A_{Burette}} \tag{13}$$

Here A_{sample} is the cross-sectional area of the sand sample holder, $A_{Burrette}$ is the cross-sectional area of the Burette and u^w_{bottom} is the Darcy water flux through the bottom.

In line with common practice, we assume that the interior sensors measure the intrinsic phase-averaged pressures, defined by:

$$p^\alpha_{in} = \frac{\int_{z_{mid}-r_{sensor}}^{z_{mid}+r_{sensor}} \omega(z)\phi S^\alpha p^\alpha dz}{\int_{z_{mid}-r_{sensor}}^{z_{mid}+r_{sensor}} \omega(z)\phi S^\alpha dz}, \qquad \omega(z) = 1-(z/r_{sensor})^2 \tag{14}$$

Here $\omega(z)$ is a geometrical factor to correct for the circular shape of the sensor. Then, the p^c_{in} will be defined as $p_{N-in} - p_{W-in}$

As indicated before, the damping coefficient τ is considered to be a function of the saturation. The dependency of this coefficient τ on the saturation is one of the research questions currently under investigation. We consider a number of possible τ-S^e relationship with the general form

$$\tau = \tau_{\max} f(S^e) \tag{15}$$

In particular, we consider the following cases:

$$f(S^e) = \begin{cases} 1 & \text{constant} \\ S^e & \text{linear} \\ (S^e)^2 & \text{quadratic} \\ \exp(-(S^e-\mu)^2/(2\sigma^2)) & \text{Gaussian} \\ (1+erf([S^e-\mu]/\sigma)/2) & \text{Error function} \end{cases} \tag{16}$$

These relations are plotted in Fig. 4.

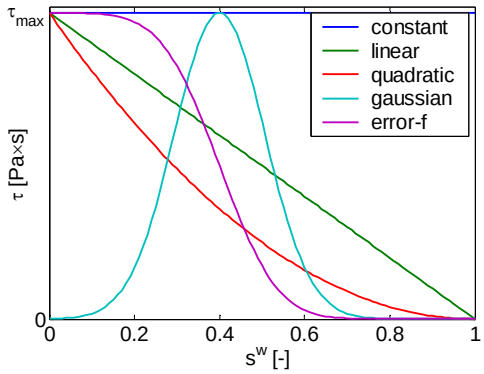

FIGURE. 4. The behaviour of the $\tau(S^e)$ relations under investigation

6. Comparison of the numerical model with the experimental data

Here we compare results of the two-phase flow numerical model with the experimental data. Table 1 shows the parameter values used in $\tau(S^e)$ formulas given in equation (16). Similar values for τ have been reported in the literature (see e.g., Gielen et al. Manthey et al., 2004, and Hassanizadeh et al., 2002). We must emphasize that we strictly focus on the qualitative behaviour of curves obtained with various models, and not on the exact agreement between simulation and experimental results.

TABLE 1: Parameter set that is used for the $\tau(S^w)$ function (eq. 16) within the non-equilibrium capillary pressure model

	Const	Linear	Quadratic	Gaussian	Error-f
τ_{max}	1e+4	3e+4	1e+5	1e+5	1e+5
μ	-	-	-	0.6	0.5
σ	-	-	-	0.15	0.2

6.1 Simulation of non-equilibrium 20-kPa experiments

First, we compare the experimental results for the 20-kPa experiment with simulation results carried out with the static capillary pressure model (i.e., τ=0), as well as two simple τ-S^e relationships, namely constant τ and the linear relation. Plots of the time rate of saturation versus saturation itself and the local dynamic capillary pressure versus sample-averaged saturation are shown in Figs 5a and 5b, respectively.

It is evident that, contrary to the measurements, the 1D static capillary pressure model predicts a monotonous behaviour. Moreover, it significantly under predicts the value of the capillary pressure. Also, Fig 5b shows that the static model gives a very wrong evolution of dS^n/dt with saturation. Thus, one may firmly conclude that the static 1D model fails to describe the physical behaviour observed in our experiments.

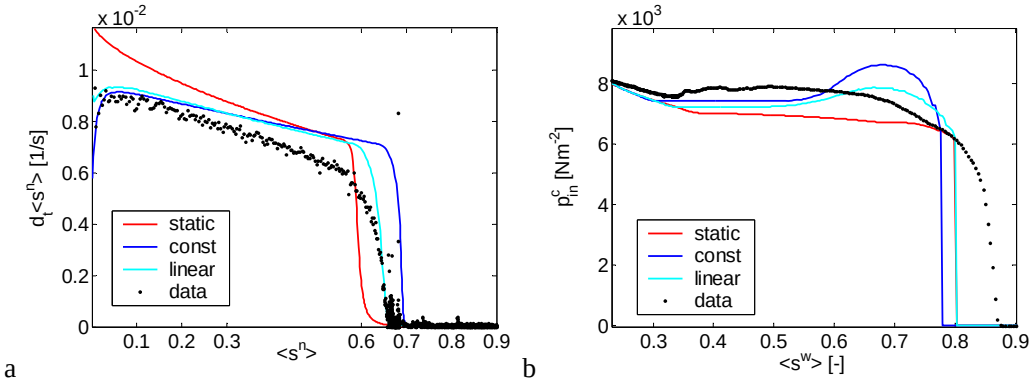

FIGURE 5 (a) the time derivative of the sample averaged DNAPL saturation versus sample averaged DNAPL saturation and (b) the interior capillary pressure as function of the sample averaged water saturation. Comparison between data of the 20kPa experiment and the two-phase flow model with static pc-s relation and two simple non-equilibrium p^c-S relations

Figs 5a and 5b show that simulation results are improved when the non-equilibrium model with constant or linear τ relation is employed, with the latter showing a better agreement with the data. However, they are both still far from providing a satisfactory fit of date points. Although they both show a non-monotonous behaviour in $p_{in}^c - \langle S^w \rangle$ curve, the overshoot occurs mainly at large water saturations, i.e. at short times. In addition, Fig 5a shows that the model with a constant τ predicts in a curve for dS^n/dt that deviates significantly from measurements at high saturations. The linear τ-S relation does a better job at early time (i.e. high saturation) constant τ case. Nevertheless, a significant deviation from data remains.

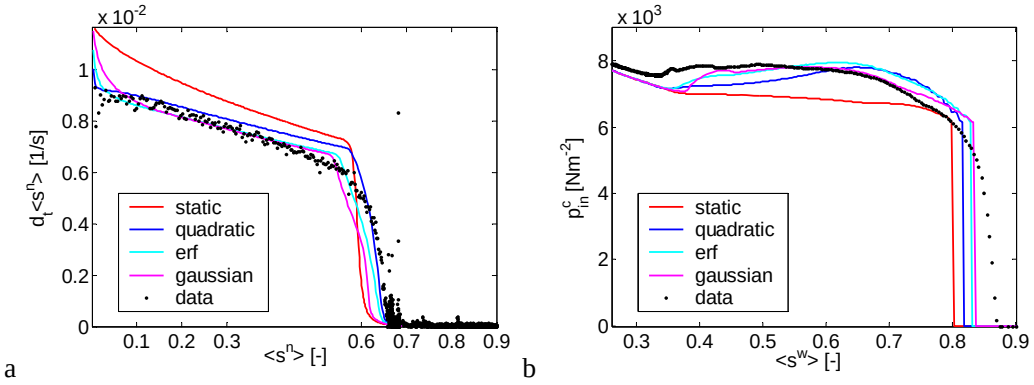

FIGURE 6 (a) the time derivative of the sample averaged DNAPL saturation versus sample averaged DNAPL saturation and (b) the interior capillary pressure as function of the sample averaged water saturation. Comparison between data of the 20kPa experiment and the two-phase flow model with static pc-s relation and the non-equilibrium model with the quadratic, exponential (μ=0.6, σ=0.15) and erf (μ=0.5, σ=0.2) τ-S relation

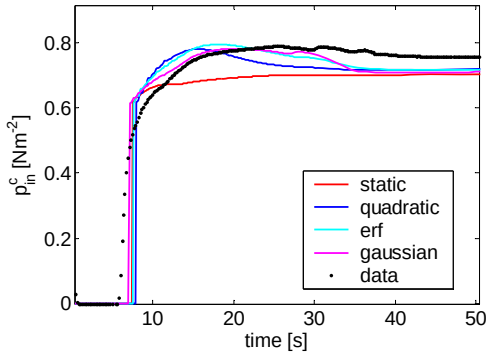

FIGURE 7 Interior capillary pressure as function of time. Comparison between data of the 20-kPa experiment and the two-phase flow model with static pc-s relation, and the non-equilibrium pc-s relation (7) for the quadratic, Gaussian and erf τ-S relations.

Next, we compare the experimental data with simulation results carried out with more complicated τ-S^e relationships, namely quadratic, error function, and Gaussian. Plots of local dynamic capillary pressure versus sample-averaged saturation, the time rate of saturation versus saturation itself, and dynamic capillary pressure versus time are shown in Figs 6a, 6b, and 7, respectively.

It is evident that all three models show considerable improvement compared to the static, constant and linear models. In particular, the error function and Gaussian relationships reproduce the non-monotonic behaviour of dynamic capillary pressure reasonably well. However, as can be seen in 7 for the capillary pressure versus time, the results are still not perfect as all models under predict the capillary pressure for intermediate times.

6.2 Simulation of non-equilibrium 16-kPa experiments

For the 16-kPa experiments, the $\partial_t < S^n > - < S^n >$ behaviour is similar as for the 20kPa experiment (see Fig 8a). The agreement between non-equilibrium models and the data for the $p_{in}^c - \langle S^w \rangle$ curve is poorer than for the 20-kPa experiment (see Fig 8b). Nevertheless, the non-equilibrium model still seems to show a major improvement over the two-phase flow model without the non-equilibrium term.

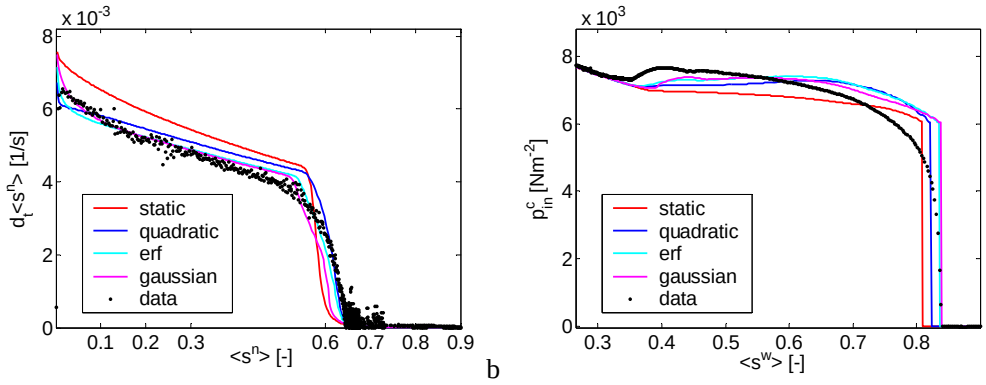

a b

FIGURE 8 (a) the time derivative of the sample averaged DNAPL saturation versus sample averaged DNAPL saturation and (b) the interior capillary pressure as function of the sample averaged water saturation. Comparison between data of the 16kPa experiment and the two-phase flow model with static pc-s relation and the non-equilibrium model with the quadratic, exponential (μ=0.6, σ=0.15) and erf (μ=0.5, σ=0.2) τ-S relation

7. Conclusions

We have performed a number of two-phase flow column experiments involving the displacement of water by PCE. Both quasi-static and dynamic capillary pressure-saturation curves have been measured. Dynamic capillary pressure-saturation curves have been obtained by measuring fluid pressures inside the soil sample. We clearly see that dynamic curves are significantly different from static curves. We have developed a two-dimensional two-phase flow model which includes the non-equilibrium (dynamic) capillary pressure theory of Hassanizadeh and Gray. The damping coefficient τ can be specified as a function of saturation using various functional forms: constant, linear, quadratic, error function, and Gaussian. We have then carried out a qualitative comparative study of experiments with the classical equilibrium capillary pressure model and the non-equilibrium capillary pressure model, employing various formulations for the damping coefficient τ.

An interesting feature of the data is that the plots of dynamic capillary pressure with time and also with saturation show a non-monotonic behaviour. We can clearly include that if we do not include the non-equilibrium capillary pressure effect in our two-phase flow model, we cannot reproduce the observed trend in experimental data. A similar conclusion was reached by O'Carroll et al. (2005) for two-phase flow in a sand column.

Inclusion of the non-equilibrium capillary pressure equation (7) improves the agreement between simulation results and data. In particular, an error function or Gaussian relationship for the damping coefficient τ provides reasonable agreement between data and simulations.

Acknowledgements

We would like to thank Mike Celia of Princeton University and Helge Dahle of Bergen University for fruitful discussions. This research has been partially supported by the Netherlands Organisation for Scientific Research (NWO). Also, support from the Utrecht Centre of Geosciences (UCG) is greatly appreciated.

References

- Barenblatt, G.I. and A.A. Gil'man (1987) "Non equilibrium counterflow capillary impregnation", Journal of engineering physics, Vol 52, p.33.
- Gielen, T.W., S.M. Hassanizadeh, M.A. Celia, Helge K. Dahle, and A. Leijnse, "A pore-scale network approach to investigate dynamic effects in multiphase flow," Proceedings of the International Conference on Computational Methods in Water Resources, Chapel Hill, North Carolina USA (June 13 - 17, 2004), Volume 1, pp. 83-94, 2004.
- Hassanizadeh, S.M and W.G. Gray (1990) "Mechanics and thermodynamics of multiphase flow in porous media including interphase boundaries," *Adv. Water Resour.*, 13, 169-186, 1990.
- Hassanizadeh, S. M. and W. G. Gray (1993) "Thermodynamic basis of capillary pressure in porous media". Water Resources Research, V29, No.10, 3389–3405.

- Helmig, R., Multiphase Flow and Transport Processes in the Subsurface, Springer, Berlin, 1997.
- Manthey, S., S.M. Hassanizadeh, O. Oung, and R. Helmig, Dynamic capillary pressure effects in two-phase flow through heterogeneous porous media, Proceedings of International Conference on Computational Methods in Water Resources, Chapel Hill, North Carolina USA (June 13 - 17, 2004), Volume 1, pp. 631-644, 2004.
- O'Carroll, D.M., T.J. Phelan and L.M. Abriola, 2005. Exploring dynamic effects in capillary pressure in multistep outflow experiments, Water Resources Research, 41, W11419, doi:10.1029/2005WR004010.